ISSN 1990-3413, Astrophysical Bulletin, 2018, Vol. 73, No. 4, pp. 401–412. © Pleiades Publishing, Ltd., 2018.
Original Russian Text © E.O. Vasiliev, M.V. Ryabova, Yu.A. Shchekinov, S.K. Sethi, 2018, published in Astrofizicheskii Byulleten', 2018, Vol. 73, No. 4, pp. 426–438.

Evolution of Intergalactic Gas in the Neighborhood of Dwarf Galaxies and Its Manifestations in the H I 21 cm Line

E. O. Vasiliev[1,2*], M. V. Ryabova[1], Yu. A. Shchekinov[3,4***], and S. K. Sethi[4****]**

[1] *Southern Federal University, Rostov-on-Don, 344090 Russia*

[2] *Special Astrophysical Observatory, Russian Academy of Sciences, Nizhnii Arkhyz, 369167 Russia*

[3] *Lebedev Physical Institute, Russian Academy of Sciences, Moscow, 199911 Russia*

[4] *Raman Research Institute, Bangalore, 560 080 India*

Received February 26, 2018; in final form, May 24, 2018

Abstract—Low-mass galaxies are known to have played the crucial role in the hydrogen reionization in the Universe. In this paper we investigate the contribution of soft x-ray radiation ($E \sim 0.1$–1 keV) from dwarf galaxies to hydrogen ionization during the initial reionization stages. The only possible sources of this radiation in the process of star formation in dwarf galaxies during the epochs preceding the hydrogen reionization epoch are hot intermediate-mass stars ($M \sim 5$–$8\ M_\odot$) that entered the asymptotic giant branch (AGB) stage and massive x-ray binaries. We analyze the evolution of the intergalactic gas in the neighborhood of a dwarf galaxy with a total mass of $6 \times 10^8\ M_\odot$ formed at the redshift of $z \sim 15$ and having constant star-formation rate of 0.01–$0.1\ M_\odot\ \mathrm{yr}^{-1}$ over a starburst with a duration of up to 100 Myr. We show that the radiation from AGB stars heats intergalactic gas to above 100 K and ensures its ionization $x_e \gtrsim 0.03$ within about 4–10 kpc from the galaxy in the case of a star-formation rate of star formation 0.03–$0.1\ M_\odot\ \mathrm{yr}^{-1}$, and that after the end of the starburst this region remains quasi-stationary over the following 200–300 Myr, i.e., until $z \sim 7.5$. Formation of x-ray binaries form in dwarf galaxies at $z \sim 15$ results in a 2–3 and 5–6 times greater size of the ionized and heated region compared to the case where ionization is produced by AGB stars exclusively, if computed with the "x-ray luminosity–star-formation rate" dependence ($L_X \sim f_X SFR$) factor $f_X = 0.1$ and $f_X \sim 1$, respectively. For $f_X \lesssim 0.03$ the effect of x-ray binaries is smaller that that of AGB star population. $Ly\alpha$ emission, heating, and ionization of the intergalactic gas in the neighborhood of dwarf galaxies result in the excitation of the 21 cm H I line. We found that during the period of the starburst end at $z \sim$11.5–12.5 the brightness temperature in the neighborhood of galaxies is 15–25 mK and the region where the brightness temperature remains close to its maximum has a size of about 12–30 kpc. Hence the epoch of the starburst end is most favorable for 21 cm H I line observations of dwarf galaxies, because at that time the size of the region of maximum brightness temperature is the greatest over the entire evolution of the dwarf galaxy. In the case of the sizes corresponding to almost $0\farcm1$ for $z \sim 12$ regions with maximum emission can be detected with the Square Kilometre Array, which is currently under construction.

DOI: 10.1134/S1990341318040028

Key words: *galaxies: dwarf—intergalactic medium*

1. INTRODUCTION

The ionization and thermal state of the background (intergalactic) gas in the pre-hydrogen ionization epoch may change because of the effect of radiation from the stellar population, x-ray sources (e.g., [1, 2]), cosmic rays [3–6], and various unstable dark-matter particles (e.g., [7–9]). The first two types of sources are believed to have dominated at redshifts starting from $z \sim 20$ to have drive hydrogen reionization (see, e.g., review [10]). Furthermore, these two sources have common origin—they are associated with stellar nucleosynthesis. The point is that x-ray sources are primarily meant to include single stellar-mass black holes and massive x-ray binaries.

Other sources of soft x-ray emission can also be found in the stellar population of present-day galax-

*E-mail: eugstar@mail.ru
**E-mail: mryabova@sfedu.ru
***E-mail: yus@asc.rssi.ru
****E-mail: sethi@rri.res.in

ies: white dwarfs, AGB stars, etc. Whereas the former need several billion years to form, stars with masses 5–8 $M_\odot$ in transition to the AGB may well form in the first protogalaxies. Note that the main-sequence lifetime of a star with such a mass is shorter and comparable to the local age of the Universe at redshifts of about 10. Therefore 100–300 eV emission of such stars may escape from the first dwarf galaxies and heat up the surrounding background gas. Note that the formation of an AGB star requires no additional assumptions, like. e.g., in the case of massive x-ray binaries, where we have to know the fraction of forming binary systems. This fraction may vary from one dwarf galaxy to another because of the small number of stars in these galaxies. Therefore the well-known relation between x-ray luminosity and star-formation rate [11] can hardly be directly applied to these objects because of the large scatter of the quantities involved. Note in this connection that although star formation in dwarf galaxies occurs in starburst modes, like in more massive galaxies, these single events lasting several tens of million years have a crucial effect on the evolution of the entire galaxy (see, e.g., [12, 13]). For example, the energy of a single starburst may be sufficient to eject most of the gas from the galaxy, and in the case of low-mass minihalos the same effect may be produced by a single supernova explosion (e.g.,[13, 14]), resulting in partial or complete suppression of star formation over the next several hundred million or several billion years. The lifetime of AGB stars is yet another fact in favor of analyzing their possible contribution to the heating of the background gas. Intermediate mass stars have a main-sequence lifetime of at least several tens of million years and therefore their effect may extend for longer time than that of x-ray binaries. On the other hand, the short-term albeit powerful effect of the latter may have longer-term consequences for the background gas because of its low density.

In this paper we analyze the effect of the sources of soft x-ray radiation in dwarf galaxies—AGB stars and massive x-ray binaries—on the ionization and thermal evolution of the intergalactic has during the epoch prior to hydrogen reionization and the observational manifestations of this effect in the H I 21-cm line. Our computations use ΛCDM model with the parameters $(\Omega_m,\Omega_b,\Omega_\Lambda,h) = (0.29,0.047,0.71,0.72)$. Section 2 describes the spectral evolution of dwarf galaxies with star formation; Section 3 briefly describes the model and the results of the computation of the ionization and thermal evolution of intergalactic gas in the galaxy neighborhoods; Section 4 analyzes the observational manifestations of the variation of the thermal evolution of intergalactic gas at the H I 21-cm line, and the final section presents the main conclusions.

2. SPECTRAL EVOLUTION OF DWARF GALAXIES

Within the framework of hierarchical clustering scenario protogalaxies with the total masses (including dark matter and gas) close to the present-day masses of dwarf spheroidal galaxies $M \sim 10^8$–$10^9\ M_\odot$ form at redshifts $z \sim 12$–15 in density perturbations corresponding to fluctuations with a magnitude of about $(3-4)\sigma$. Note that first stars begin to form a little earlier, $z \sim 20$, in the dark-matter halo with a mass of $M \sim 10^5$–$10^7\ M_\odot$ [15–18], and their evolution may result in effective sweep-up of gas from the host halo (see, e.g., [13]). Thus during further mergers these halos increase insignificantly the mass of gas as a result of the formation of dwarf galaxies. However, this gas may evidently be enriched in heavy elements or metals thereby promoting the formation of low-mass stars in dwarf protogalaxies. Note that the evolution of massive stars with zero metallicity does not bring about significant mass loss by the halos with masses greater than $M \sim 10^7\ M_\odot$, i.e., explosions of first supernovae would enrich their host galaxies with metals [19, 20].

In most of the present-day galaxies with masses $M \sim 10^8 - 10^9\ M_\odot$ multiple stellar populations have been found, which are distinctly separated in age. Note that the ages of the oldest stars are greater than the time elapsed since the hydrogen reionization epoch (see, e.g., [21]). These observations allow reconstructing the star formation history in dwarf galaxies, which includes two or three significant starbursts. During the first starburst, which proves to be the most intense, the star formation rate remains practically constant in the interval from several tens to several hundred million years, and its value may lie in the broad interval $SFR \sim 10^{-3} - 0.1\ M_\odot\ \mathrm{yr}^{-1}$. The effect of this burst of star formation on the interstellar gas proves to be sufficient to suppress star formation processes for a long time and the next star-formation burst usually occurs after several billion years.

We use PEGASE package [22] to compute the chemical evolution and obtain that with a constant star-formation rate equal to the upper limit of $0.1\ M_\odot\ \mathrm{yr}^{-1}$ over 100 Myr the average metallicity of stars by the end of the starburst would not exceed $[Z/H] \sim -1$, which is quite compatible with the evolutionary models and observations of present-day dwarf galaxies (e.g.,, [23]). In the case of higher star-formation rate frequent supernova explosions may result in effective gas loss by the galaxy during the very first several million years and hence the chemical evolution model that we employ take this gas loss into account.

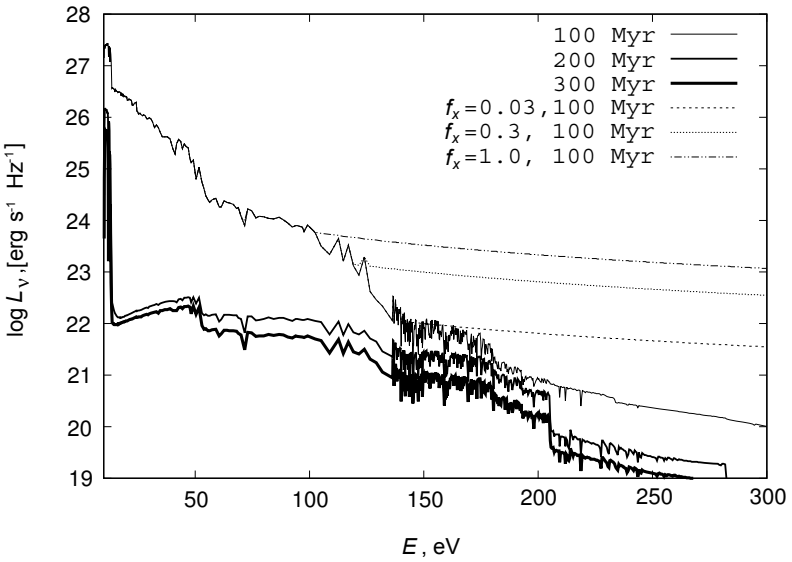

Fig. 1. Spectral luminosity of the stellar population with the age of 100, 200, and 300 million years (the thick solid lines going from top to down) in a galaxy with an initial gas mass of $M_0 = 10^8 M_\odot$ and constant star-formation rate of $SFR = 0.1\ M_\odot\ \mathrm{yr}^{-1}$ over the first 100 Myr. The dashed, dotted, and dashed-and-dotted lines show the spectra for the time of the end of the starburst computed with the account taken of the radiation of massive x-ray binaries with the correction factor of $f_X = 0.03$, 0.3, and 1, respectively.

Our computations showed that in the case of star-formation rate lower than $SFR \sim 0.01\ M_\odot\ \mathrm{yr}^{-1}$ the flux is too weak for any appreciable heating of gas at distances greater than 2–3 virial radii for galaxies with masses $M \sim 10^8$–$10^9\ M_\odot$. For this reason we restrict our analysis to the star-formation rate interval 0.01–$0.1\ M_\odot\ \mathrm{yr}^{-1}$ and adopt the upper limit as the standard value. For the sake of definitiveness we consider the chemical and spectral evolution of a dwarf galaxy with a total mass of $M = 6 \times 10^8\ M_\odot$ and initial gas mass of $M_0 = (\Omega_b/\Omega_m)M = 10^8\ M_\odot$ that formed at the redshift of $z = 15$ and has a constant star-formation rate over 100 Myr. Fig. 1 shows the spectral dependence of the stellar population with the age of 100, 200, and 300 Myr in such a galaxy with a star-formation rate of $SFR = 0.1\ M_\odot\ \mathrm{yr}^{-1}$. By the end of the starburst, $t = 100$ Myr, the spectrum is dominated by photons with energies 13.6–100 eV emitted by massive stars, which are to explode as supernovae in about 10–20 Myr. Afterwards, without further star formation, the luminosity in this part of the spectrum drops by several orders of magnitude over the following 10–20 Myr and then slowly decreases over several hundred million years.

In about 30 Myr after the beginning of the starburst stars with masses of about $8\ M_\odot$ start to evolve away from the MS toward the AGB. Stars at this stage become sufficiently hot to emit photons with energies 100–300 eV. The spectral libraries used in PEGASE program are limited by the 91Å wavelength (corresponding to the energy of 136 eV) and therefore in our computations we replaced the spectral library [24] for hot stars by the corresponding library from [25], which has a much higher limiting energy of about 2 keV. As it is evident from Fig. 1, the spectrum in the 100–300 eV energy interval varies less than by one order of magnitude over a time span of several million years. Extension of the spectrum mostly results in a significant increase of ionization and heating by secondary electrons from soft x-ray photons in the model without x-ray binaries.

In the process of star formation binary stars may form, which then become massive x-ray binaries. For present-day galaxies with ongoing star formation an empirical relation is established between the star-formation rate and x-ray luminosity provided by the radiation of x-ray binaries [11]:

$$L_X = 3.4 \times 10^{40} f_X \left(\frac{SFR}{1 M_\odot \mathrm{yr}^{-1}} \right) \mathrm{erg\,s}^{-1}, \quad (1)$$

where f_X is the correction factor, which is equal to 0.3–1 [11, 26] for galaxies in the local universe, but generally may differ for galaxies at large redshifts. For example, CHANDRA observations suggest that a possible value of $f_X \gtrsim 2 - 5$ for galaxies at $z \sim 6$ [27]. Note that in this case bright massive galaxies were evidently observed with star-formation rates higher than in nearby galaxies. In our model we consider dwarf galaxies with low star-formation rates and small stellar masses, and therefore their f_X

factor can hardly be higher than its typical values for local galaxies, or maybe even lower. Fig. 1 shows, by way of an example, the spectra for several f_X factor values at the time of 100 Myr. Immediately after this time star formation ceases in our galaxy model and the contribution of x-ray binaries becomes equal to zero, implying that $f_X = 0$ at later time instants. It goes without saying that such stars do not vanish immediately, but the time lag may amount to about 30 Myr—the lifetime of the donor star in the binary system. This time has little effect on our results. It is evident from Fig. 1 that in the case of small f_X the emission of x-ray binaries dominates at energies above 100–150 eV. These very photons, which are produced by massive x-ray binaries , easily escape from dwarf galaxies and heat up the ambient gas (e.g., [28]).

During the star-formation stage the stellar population of dwarf galaxies emits a huge number of $Ly\alpha$-photons. The spectral luminosities $L(Ly\alpha)$ for a star-formation rate of 0.1 $M_\odot$ yr^{-1} by the end of the burst of star formation turns out to be higher than 10^{27} erg s^{-1} Hz^{-1} (Fig. 1). Given the large optical depth at the $Ly\alpha$ line center, which exceeds 10^5 inside the galaxy, the number of absorptions should equal the number of emissions. Therefore the $Ly\alpha$ flux at the distance of r from the galaxy can be estimated as $F(Ly\alpha) = L(Ly\alpha)/4\pi r^2$. For example, the flux of $Ly\alpha$ photons at the distance of 1 kpc from the center of a galaxy with the initial gas mass of $M_0 = 10^8 M_\odot$ and constant star formation rate of 0.1 $M_\odot$ yr^{-1} by the end of the burst of star formation, i.e., by 100 Myr, is equal to 10^{-16} erg s^{-1} cm^{-2} Hz^{-1} sr^{-1}, but decreases by more than by one order of magnitude after 40 Myr, and by almost a factor of 300 within 100 Myr after the end of the starburst (we do not show the part of the spectrum with the $Ly\alpha$ flux in Fig. 2 because of the very large interval spanned by this quantity).

The first massive stars emit sufficient number of ionizing photons, which can ionize the gas inside the dwarf galaxy (e.g., [29–31]) and contribute to the escape of a part of the photons from the host galaxy. The escape of photons is then facilitated by SN explosions, which produce cavities of hot gas comparable in size with the virial radius of the galaxy (e.g., [12–14]). Thus several massive stars and several SN explosions within 10–20 Myr may ionize appreciably the central, densest part of the dwarf galaxy and facilitate the escape of photons from the next stellar population. Note that appreciable part of neutral gas remains inside the galaxy, both at its periphery and in the overlapping shells of supernova ionization zones. If the star-formation rate remains sufficiently low to allow the formation of a sufficient number of SNs for the sweepout of the bulk of the gas from the galaxy, the average hydrogen column density in the interstellar medium can be expected to be quasi-stationary. Therefore for the sake of simplicity we assume that the column density of atomic hydrogen $N_{\rm H\,I}$ inside the galaxy remains constant inside the galaxy during its evolution. Let us now consider the evolution of the spectral flux emerging from the galaxy for two column-density values: $N_{\rm H\,I} = 10^{19}$ cm^{-2}

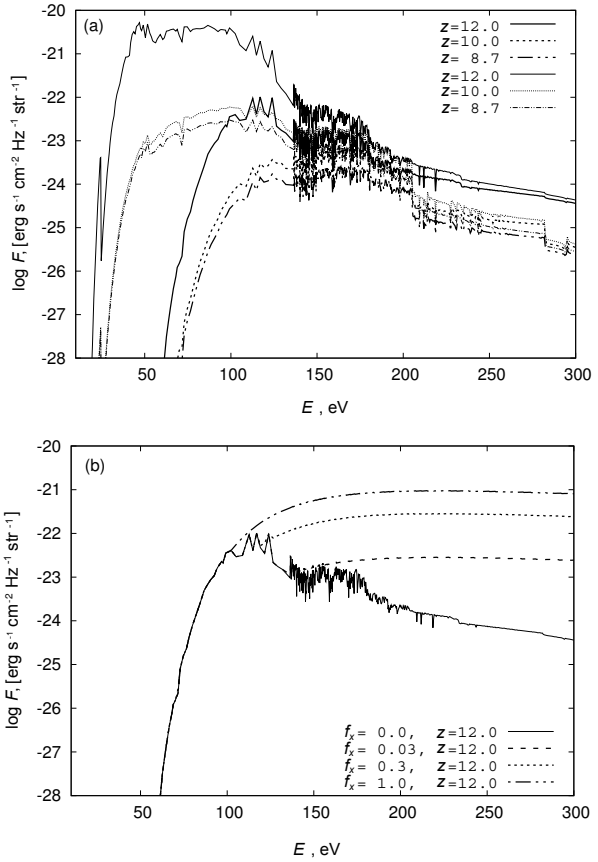

Fig. 2. a) Spectral flux of [ionizing] radiation at a distance 1 kpc from the center of a galaxy with an initial gas mass $M_0 = 10^8 M_\odot$ and star-formation rate $SFR = 0.1\ M_\odot$ ye^{-1}, which remains constant over the first 100 My and which began at the redshift of $z = 15$, for two values of hydrogen column density inside the galaxy: $N_{\rm H\,I} = 10^{19}$ cm^{-2} (the thin solid lines) and $N_{\rm H\,I} = 10^{20}$ cm^{-2} (the thick solid lines). The solid, dashed, and dotted lines show the spectral fluxes from the stellar population with the age equal to 100, 200, and 300 million years, which corresponds to the redshifts of $z = 12$, 10, and 8.7, respectively. b) Spectral flux of ionized radiation of the stellar population at a distance of 1 kpc from the center of a galaxy with the parameters indicated above and with the age of 100 Myr computed with the allowance for the contribution from massive x-ray binaries: $f_X = 0$ (the solid line), $f_X = 0.03$ (the dashed line), $f_X = 0.3$ (the dotted line), and $f_X = 1$ (the dashed-and-dotted line).

and 10^{20} cm^{-2}. Note that for the for the total mass values of ($M \sim 10^8$–$10^9 M_\odot$) and the formation time ($z \sim 10 - 15$) of the dwarf galaxy the second $N_{\rm H\,I}$ value is only a factor of 1–3 lower than the limiting value for the fully ionized plasma: $N^*({\rm H\,I}) \sim \langle n \rangle r_v$, where $\langle n \rangle \simeq 200 n_b(z_v)$ is the virial gas density inside the protogalaxy; $n_b(z_v)$, the background gas density at redshift z_v at which the virialization occurred, and r_v is the virial radius of the galaxy.

Fig. 2a shows the spectral flux of ionized radiation from the stellar population at a distance of 1 kpc from the center of the galaxy, i.e., beyond the virial radius of a galaxy with the total mass of $M = 6 \times 10^8 M_\odot$. We assumed the star-formation rate to be constant and equal to 0.1 $M_\odot$ yr^{-1} over the first 100 Myr starting from $z = 15$. The H I column density inside the galaxy remained equal to $N_{\rm H\,I}$ during the evolution. Fig. 2 shows the spectral fluxes of ionizing radiation for two $N_{\rm H\,I}$ column-density values: 10^{19} cm^{-2} (the thin solid lines) and 10^{20} cm^{-2} (the thick solid lines). It is easy to see that in the case of higher $N_{\rm H\,I}$ photons with energies below 100 eV are efficiently absorbed inside the host galaxy, and the escaping photons are those produced by hot AGB stars and/or x-ray binaries. Note that the latter source dominates at $f_X \gtrsim 0.03$ (Fig. 2b).

Thus the spectral flux of ionizing radiation at a distance of r from the dwarf galaxy is equal to:

$$F_\nu = \frac{L_\nu}{4\pi r^2} \exp(-\tau_{\rm h}) \exp(-\tau_{\rm IGM}) \qquad (2)$$

where the first exponential factor is associated with absorption inside the galaxy: $\tau_{\rm h} \sim N^h_{\rm H\,I}$, where $N^h_{\rm H\,I}$ is the H I column density inside the galaxy and which we assume to be constant, and the second exponential factor is determined by the absorption in the surrounding gas and depends on its ionization history.

3. IONIZATION AND THERMAL EVOLUTION OF INTERGALACTIC HAS IN THE NEIGHBORHOOD OF DWARF GALAXIES

Let us now consider the ionization and thermal evolution of gas in concentric spherical shells centered on a dwarf galaxy. The radii of the shells lie in the interval from 10^3 to 5×10^5 pc and the radii of the neighboring shells differ by a factor of $a_r = 1.11$ so that $r_{i+1} = a_r r_i$. As a result, the total number of shells for the given interval of distances is of about 60 (the choice of the number of shells is determined by the smoothness of the derived dependences of physical quantities and speed of computations). Note that the radius of the inner shell is greater by about 20% than the virial radius of the galaxy with a total mass of $M = 6 \times 10^8 M_\odot$ that formed at $z = 15$ (e.g., [32]). There is a transition region between the galaxy and intergalactic gas with a complex distribution of density, temperature, and gas velocity. However, the density and temperature of matter at the virial radius are close to their background values. In our computations we set the inner radius close to the virial radius. Because of the small difference between the virial radius and the inner radius of the shell and low gas density in the neighborhood of the virial radius this region produces the minimum contribution to the total absorption. We can thus start our computations for background gas outside the dwarf galaxy. We assume, for the sake of simplicity, that the background gas is distributed uniformly and that its density and temperature vary as $(1+z)^3$ and $(1+z)^2$, respectively.

For each spherical shell we solve the set of ionization kinetics and thermal evolution equations for the hydrogen-and-helium plasma. These equations include all the main processes occurring in matter with primordial chemical composition, in particular, collisional ionization and recombination for H I, H II, He I, He II, He III, and e^-, photoionization caused by the ultraviolet and x-ray radiation of the stellar population absorbed both inside the protogalaxy and by the background intergalactic gas. The equation for temperature includes the cooling processes determined by collisional ionization of H I, He I, He II, recombination of H II, He II (both radiative and dielectronic) and He III, collisional excitation of H I, He I (1^2S and 2^3S), He II, free-free transitions, and heating due to the Compton process and photoionization. We adopt the chemical-reaction and cooling/heating rates from [33, 34]. Here we consider ionization by x-ray radiation and therefore have to take into account the effect of secondary electrons [35, 36]. We have also to include the term responsible for the adiabatic cooling due to the Hubble expansion of the Universe into the temperature equation because we consider the evolution of the background gas on time scales exceeding the local age of the Universe. We compute the initial levels of the temperature and hydrogen ionization degree via RECFAST program [37]. We also assume that helium is initially totally neutral.

Fig. 3 shows the radial distributions of the temperature and relative H II ion density (the top and middle panels) around the galaxy with an initial gas mass of $M_0 = 10^8 M_\odot$ and constant star-formation rate $SFR = 0.03\ M_\odot$ yr^{-1} (the thin black lines) and 0.1 $M_\odot$ yr^{-1} (the thick gray lines) over the first 100 Myr starting from the redshift of $z = 15$. We set the H I column density inside the galaxy equal to $N_{\rm H\,I} = 10^{20}$ cm^{-2}. Note, in the first place, that the

temperature and hydrogen ionization profiles after $z \lesssim 12$ depend only slightly on time over almost 200 Myr, or, in other words, the partial ionization region around the galaxy with $SFR \sim 0.03$–$0.1\ M_\odot\ \mathrm{yr}^{-1}$ is quasi-stationary. This is indicative of the steady-state quasi-equilibrium between ionization and recombination, heating and cooling. Note two features for the case of the star-formation rate of $0.1\ M_\odot\ \mathrm{yr}^{-1}$. First, most of the hydrogen inside the inner region at distances $r \sim 1$–20 kpc remains neutral: $x_{\mathrm{H\,II}} \sim x_{\mathrm{H\,I}} \sim 0.5$ despite the high temperature $T \sim 10^4$ K in this region, which is a consequence of the preceding nonstationary ionization. Second, the ionization degree at small distances decreases slightly in the course of evolution (decrease of z), and this decrease is due to the decrease of the temperature and slight increase at greater distances due to ionization by secondary electrons.

Decreasing the absorption of ionizing photons inside the galaxy down to $N_{\mathrm{H\,I}} = 10^{19}\ \mathrm{cm}^{-2}$ within $r \lesssim 3$ kpc results in the increase of the ionization degree of the intergalactic gas almost to 99% by $z \sim 12$, however, after the burst of star formation ends hydrogen recombines to $x_{\mathrm{H\,I}} \sim 0.3$ by $z \sim 11$ and remains at this level for the next 200–300 Myr, i.e., to $z \sim 7.5$. The size of the region where the ionization degree exceeds the residual value of $x_e \sim 2 \times 10^{-4}$, depends only slightly on the column density inside the galaxy because partial ionization at large galactocentric distances is driven by x-ray radiation.

The birth of massive x-ray binaries in the process of star formation changes substantially the sizes of ionized gas regions in the neighborhood of dwarf galaxies. The dynamics of this process was analyzed in papers [28, 38] and therefore here we only point out a few important features. The ionization degree of intergalactic gas near galaxies increases compared to the case when it is caused by the radiation of soft x-ray photons by AGB stars exclusively, however, even at $f_X \sim 1$ $x_{\mathrm{H\,II}}$ does not exceed 0.8 for H I column densities $N_{\mathrm{H\,I}} = 10^{20}\ \mathrm{cm}^{-2}$ inside the galaxy. The region around the galaxy where the ionization degree exceeds its residual level also increases compared to the case $f_X = 0$, where this region has the size of $r \sim 100$ kpc (see Fig. 3): the size increases by a factor of about 1.5–2 and 5–6 for $f_X \sim 0.03$ and $f_X \sim 1$, respectively. Note that this size remains almost unchanged after $z \simeq 12$ over several hundred million years, and the maximum ionization degree in the inner region (the one that is closer to the galaxy) proves to be on the same order of magnitude as the relative H I concentration: $x_{\mathrm{H\,II}} \sim x_{\mathrm{H\,I}} \sim 0.5$, like in the case where ionization is caused by AGB stars exclusively (Fig. 3).

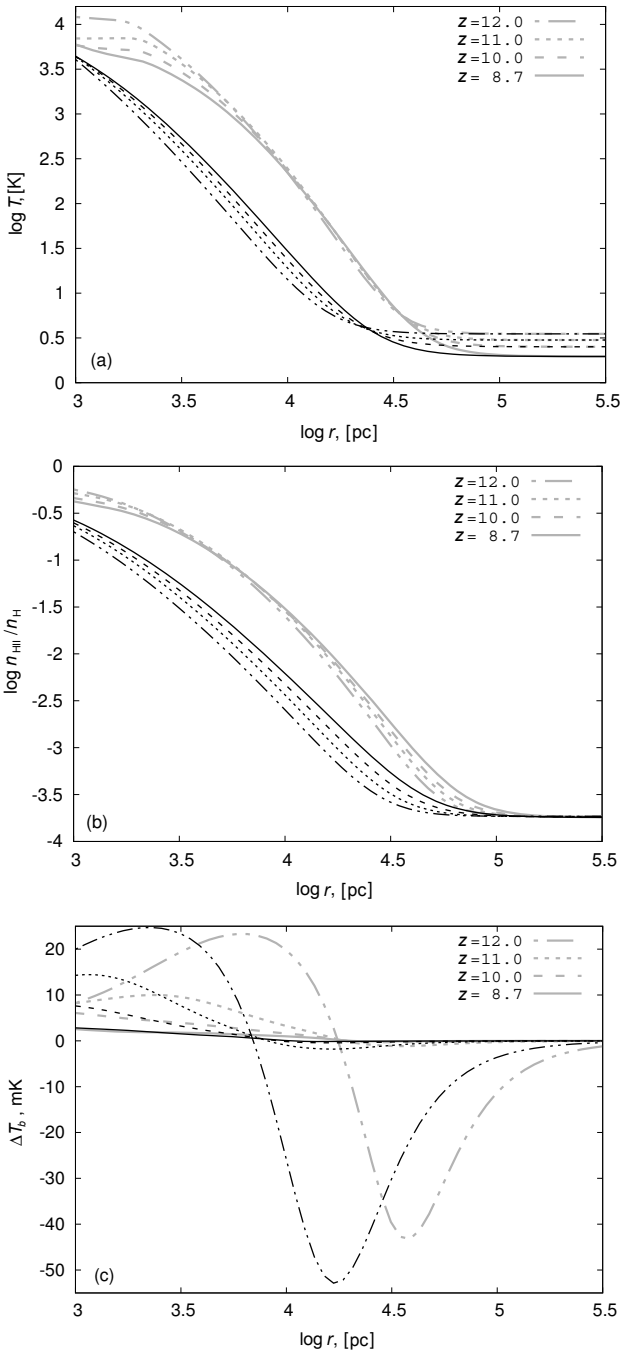

Fig. 3. Radial distributions of temperature (panel (a)), relative H II concentrations (panel (b)), and the 21-cm neutral-hydrogen line brightness temperature (panel (c)) around a galaxy with the gas mass of $M_0 = 10^8 M_\odot$ and constant star-formation rate $SFR = 0.03\ M_\odot\ \mathrm{yr}^{-1}$ (the thin black lines) and $0.1\ M_\odot\ \mathrm{yr}^{-1}$ (the thick gray lines) during the first 100 million years starting at $z = 15$. The solid, dashed, and dotted (or dashed-and-dotted) lines show the distributions at redshifts $z = 12$, 11, 10, and 8.7, which corresponds to the age of the stellar population in the galaxy of about 100, 140, 200, and 300 Myr. We assumed that the H I column inside the galaxy remains equal to $N_{\mathrm{H\,I}} = 10^{20}\ \mathrm{cm}^{-2}$.

4. EMISSION PROPERTIES

Incomplete hydrogen ionization ($x_{\rm H\,I} \gtrsim 0.3$) and appreciable heating of intergalactic gas ($T \gtrsim 100$ K) in the neighborhood of dwarf galaxies during and after the burst of star formation should definitively result in the excitation of the H I 21-cm line and, given that the spin temperature [39, 40]

$$T_s^{\rm H\,I} = \frac{T_{\rm CMB} + y_a T + y_c T}{1 + y_a + y_c} \qquad (3)$$

is higher than the cosmic microwave background temperature, gas in the optically thin case should emit in the H I 21-cm line with a brightness temperature of [41, 42]

$$\Delta T_{21}^b = 25\ {\rm mK}\ (1+\delta)\ \frac{n_{\rm H\,I}}{n}\ \frac{T_s^{\rm H\,I} - T_{\rm CMB}}{T_s^{\rm H\,I}} \left(\frac{\Omega_b h}{0.03}\right) \times \left(\frac{0.3}{\Omega_m}\right)^{0.5} \left(\frac{1+z}{10}\right)^{0.5} \left[\frac{H(z)/(1+z)}{dv_{||}/dr_{||}}\right], \qquad (4)$$

where δ is the density excess over the background level. We analyze the evolution of uniform background gas and therefore $\delta = 0$. For the same reason we adopt here uniform Hubble expansion, implying that the gradient of the motion of gas along the line of sight $dv_{||}/dr_{||}$ is equal to $H(z)/(1+z)$. Variation of the spin temperature may be caused by the pumping of $Ly\alpha$ photons [39, 40] and collisions with hydrogen atoms [43] and electrons [44]. The pumping rate is determined by the background intensity of the $Ly\alpha$ emission from the stellar population of the host galaxy and locally injected photons from recombinations [41, 45]. We adopt the $Ly\alpha$ luminosities of the stellar population of the galaxy from the stellar evolutionary computations performed using PEGASE package (Fig. 1). In the case of partial ionization and heating of gas by soft x-ray photons up to 40% of their initial may be transferred to $Ly\alpha$ photons [36, 46], i.e., these photons are additionally injected into the line center.

The bottom panel in Fig. 3 shows the radial brightness temperature distributions in the H I 21-cm line around a galaxy with an initial gas mass of $M_0 = 10^8 M_\odot$ and constant star-formation rate over the first 100 Myr starting at the redshift of $z = 15$. We set the H I column density inside the galaxy equal to $N_{\rm H\,I} = 10^{20}$ cm^{-2}. Brightness temperature near the galaxy is positive, reaches its maximum $\Delta T_b \sim 25$ mK by the end of the burst of star formation at $z = 12$, and decreases almost down 1.5–2 mK by $z \sim 9$. This decrease is due to the decrease of the flux of $Ly\alpha$ photons from the stellar population after the end of the process of star formation. During star formation and in the following epoch, i.e., at $z \gtrsim 11$, the main contributors to the excitation of the line are $Ly\alpha$ photons whose flux decreases both in the process of the evolution and with the distance from the galaxy. Collisions become the dominating source of excitation at small redshifts and large distances.

For the star-formation rate equal to 0.1 $M_\odot$ yr^{-1} (the thick gray lines) the brightness temperature reaches its maximum at a distance of $r \sim 3$ kpc and remains positive with the sphere $r \lesssim 20$ r. The decrease of the star-formation rate down to 0.03 $M_\odot$ yr^{-1} (the thick black lines) result in the decrease of the size of the maximum-emission region to only twice the virial radius. Note that the maximum of the brightness temperature does not only decrease but also shifts toward smaller distances from the galaxy, reaching the minimum radius at $z \sim 9$ in our computations.

The gas temperature decreases with the distance from the galaxy and becomes lower than the temperature of cosmic background radiation. Under these circumstances the brightness temperature becomes negative—gas absorbs radiation in the H I 21-cm line. In the case of significant flux of $Ly\alpha$ photons the absorption properties of the partially ionized and substantially heated gas are changed significantly. The bottom panel in Fig. 3 shows that at redshift $z = 12$ the brightness temperature at distances greater than 20 kpc around a galaxy with the star-formation rate equal to 0.1 $M_\odot$ yr^{-1} is negative and reaches minimal values of almost -40 mK at a distance of $r \sim 30$ kpc, which is a manifestation of the effect of $Ly\alpha$ photons. For the lower star-formation rate 0.03 $M_\odot$ yr^{-1} the size of the absorption region is about twice smaller. In the process of the evolution the temperature of cosmic background radiation gradually decreases and so does the difference $T_s^{\rm H\,I} - T_{\rm CMB}$ in (4). Furthermore, after star formation ends in the host galaxy the flux of $Ly\alpha$ photons decreases. Because of these two factors absorption decreases substantially at lower redshifts.

Note that in the case of the star-formation rate 0.01 $M_\odot$ yr^{-1} the temperature and ionization degree of gas remain at their residual levels after the recombination epoch, $x_e \sim 2 \times 10^{-4}$, for almost 100 Myr after the beginning of the burst of star formation, i.e., in the redshift interval from 15 to 12. The temperature near the shell with the minimum radius considered in the model, $r \sim 10^3$ pc, then increases to 10^3 K, and the ionization degree, to 0.1. In this sense the star-formation rate value of 0.03 $M_\odot$ yr^{-1} proves to be critical for conditions necessary for the emergence of appreciable H I 21-cm line emission.

The decrease of the absorption of ionizing radiation inside the galaxy causes the expansion of the ionization regions and heats gas in their vicinity and

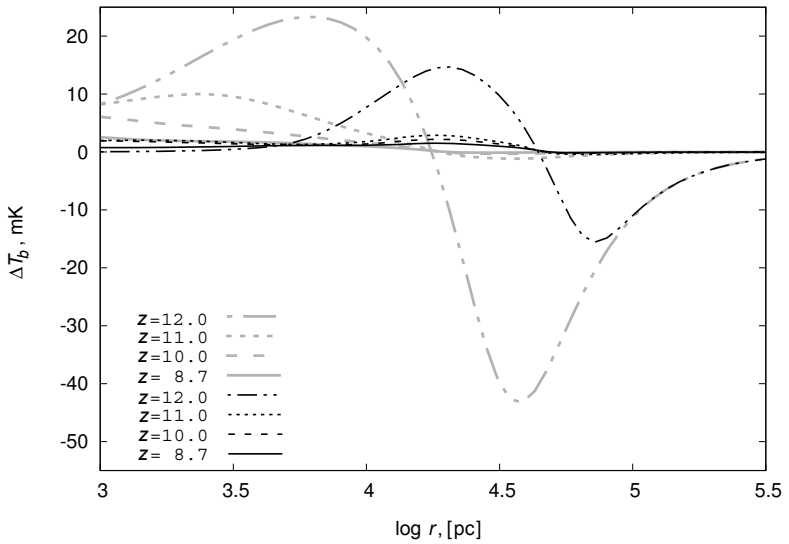

Fig. 4. Radial brightness temperature profiles of the H I 21-cm line around a galaxy with the initial gas mass of $M_0 = 10^8 M_\odot$ and a constant rate of star formation $SFR = 0.1\ M_\odot\ \mathrm{yr}^{-1}$ during the first 100 Myr that at the redshift of $z = 15$, for two values of H I column density inside the galaxy: $N_{\mathrm{H\,I}} = 10^{20}\ \mathrm{cm}^{-2}$ (the thick gray lines) and $N_{\mathrm{H\,I}} = 10^{19}\ \mathrm{cm}^{-2}$ (the thin black lines). The solid, dashed, dotted and dashed-and-dotted lines show the distributions at the redshifts of $z = 12$, 11, 10, and 8.7, which correspond to the stellar-population ages of about 100, 140, 200, and 300 Myr.

hence results in the increase of the size of the emission region in the H,I 21 cm line. For example, Fig. 4 shows the brightness temperature profiles in the 21-cm line for the H I column density $N_{\mathrm{H\,I}} = 10^{19}\ \mathrm{cm}^{-2}$ inside the galaxy (the thin black lines). Inside the radius $r \sim 3$–4 kpc gas is fully ionized and hence the signal in the 21-cm line is equal to zero. Beyond this radius the region of partial ionization and heating is located, where gas is heated above the cosmic-background-radiation temperature and can be detected in emission. Evidently, the distance from the galaxy where the brightness temperature reaches its maximum increased by a factor of 3 compared to the corresponding distance for $N_{\mathrm{H\,I}} = 10^{20}\ \mathrm{cm}^{-2}$ (the thick gray lines). The signal level decreased almost twice down to about 14 mK due to the decrease of the flux of $Ly\alpha$ photons with distance. The same factor explains the decrease of the absorption efficiency in the 21-cm line at the periphery of the region of influence, where the gas temperature is lower than the temperature of cosmic background radiation: the minimum brightness temperature is of about -15 mK.

A similar pattern shows up if we increase the flux of photons with energies above 100 eV emitted by massive x-ray binaries (Fig. 2). Fig. 5 shows the evolution of the brightness temperature at the H I 21-cm line for the gas located in the radiation field of both the stellar population with AGB stars exclusively and from x-ray binaries during the burst of star formation and during a short time after the burst for the standard H I column density inside the galaxy $N_{\mathrm{H\,I}} = 10^{20}\ \mathrm{cm}^{-2}$ adopted here. In the case of $f_X < 0.03$ the brightness temperature reaches its maximum almost at the same distance from the galaxy as in the case where ionization is produced by AGB stars exclusively. The growth of f_X increases the flux of x-ray photons (see Fig. 2) and substantially expands the region of heated gas (see the discussion in the next paragraph), which shows up in the shift of the position of the brightness-temperature maximum further away from the galaxy: for $f_X \sim 1$ the maximum is located at the distance of $r \sim 18$ kpc, which is a factor of 3 farther from the galaxy than in the case where ionization is caused by AGB stars exclusively. More efficient heating of the gas by the radiation from x-ray binaries reduces absorption in the line at the periphery of the region of influence by the end of the burst of star formation: the minimum brightness temperature at $z = 12$ increases from about -40 mK for $f_X = 0$ to almost -3 mK for $f_X = 1$.

Let us now consider the evolution of the radii of the regions around the galaxy with ongoing star formation, inside which the intergalactic gas is heated above a certain limit. Fig. 6 shows the radii of the spherical regions inside which the gas temperature is higher than 10^3 K (the dashed line), 10^2 K (the dotted line), and higher than the temperature of cosmic microwave background $T_{\mathrm{CMB}}(z)$ (the dashed-and-dotted line), and the galactocentric distance where the brightness temperature in the H I 21-cm line reach sits maximum (the solid line). While star for-

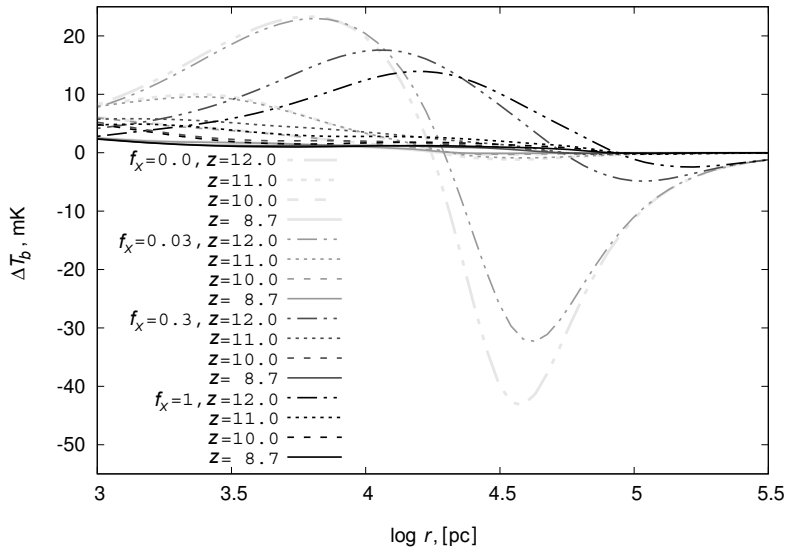

Fig. 5. Radial profiles of the brightness temperature in the H I 21-cm line around a galaxy with the initial gas mass of $M_0 = 10^8 M_\odot$ and constant star-formation rate $SFR = 0.1\ M_\odot\ \mathrm{yr}^{-1}$ over the first 100 Myr starting at the redshift of $z = 15$ including the contribution from massive x-ray binaries: $f_X = 0$, 0.03, 0.3 and 1 (from the light-gray to the black line). The solid, dashed, dotted, and dashed-and-dotted lines show the distributions at the redshifts of $z = 12$, 11, 10, and 8.7, which correspond to the galaxy stellar-population ages of about 100, 140, 200, and 300 Myr. We set the H I column density inside the galaxy equal to $N_{\mathrm{H\,I}} = 10^{20}\ \mathrm{cm}^{-2}$.

mation goes on in the host galaxy the radii of the regions with $T \gtrsim 10^3$ K practically coincide with the radii of the regions with maximum brightness temperature. After the end of the burst of star formation the dependence on the efficiency of absorption of radiation in the host galaxy shows up. In the case of the H I column density $N_{\mathrm{H\,I}} = 10^{20}\ \mathrm{cm}^{-2}$ the flux of ionizing radiation proves to be insufficient to sustain the ionization region around the galaxy, and gas at a distance of several kpc begins to recombine (see the top and middle panels in Figs. 3). This shows up in the shift of the brightness-temperature maximum toward smaller distances, which can be seen in the bottom panel in Fig. 3 and is clearly seen in the top left panel in Fig. 6. If the column density is decreased down to $N_{\mathrm{H\,I}} = 10^{19}\ \mathrm{cm}^{-2}$ then the flux of ionizing radiation becomes sufficient to sustain an extended ionization region around the galaxy. Under these conditions the maximum of the brightness temperature barely shifts toward smaller radii, although it decreases in the process of evolution, as it is noticeable in Fig. 4 and can be clearly seen in the top right panel in Fig. 6.

The increased effect of x-ray binaries results in the increase of the distances where the brightness temperature reaches its maximum, however, after the burst of star formation ends then size of the region decreases within the same time scale, which is equal to about 40–50 Myr. This can be seen from a comparison of the top and bottom panels in the left-hand column in Fig. 6, where the sizes of the regions are shown for $f_X = 0$ and 0.3, respectively.

Note that within the region with $T > 100$ K one might expect nonzero brightness temperature. The radii of the regions with temperatures above a certain level evolve in a similar way: their sizes increase during the burst of star formation , gradually reaching their maximum values, and when star formation ends these regions cease to grow and in some cases even shrink, which is due to recombination. However, this decrease is insignificant and the size of the region of influence can be assumed to remain constant after the end of star formation.

Thus, the galactocentric distance, where the brightness temperature reaches its maximum, increases in the process of star formation and then decreases or remains almost constant depending on the absorption of ionizing radiation in the host galaxy. It is easy to find the interval of redshifts where the size of the region of maximum brightness temperature is the largest during the evolution. For better visualization we show in the bottom right panel in Fig. 6 the evolutionary (redshift) dependences of the maximum brightness temperature in the H I 21-cm line on galactocentric distance where this maximum is reached for models with $f_X = 0, 0.3$, and 1 with $N_{\mathrm{H\,I}} = 10^{20}\ \mathrm{cm}^{-2}$ and for model $f_X = 0$ with $N_{\mathrm{H\,I}} = 10^{19}\ \mathrm{cm}^{-2}$. Each evolutionary track starts in the top left part of the diagram and redshift varies along the lines in the clockwise direction and is shown

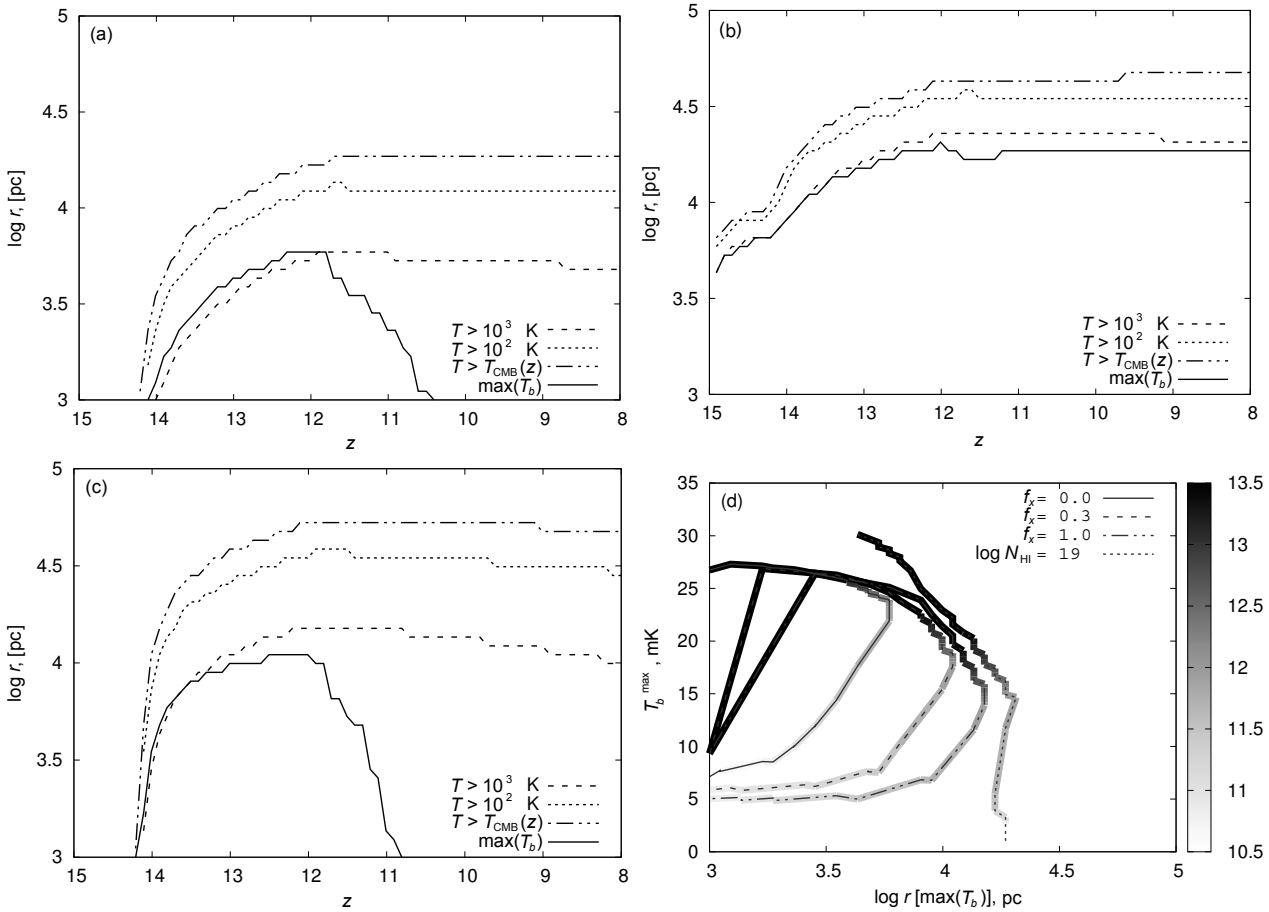

Fig. 6. The radius of the same spherical regions around the galaxy as in Figs. 4–5, inside which the gas temperature is higher than 10^3 K (the dashed line), 10^2 K (the dotted line), and than the temperature of cosmic background radiation $T_{\rm CMB}(z)$ (the dashed-and-dotted line), and the galactocentric distance where the brightness temperature in the H,I 21-cm line reaches its maximum (the solid line). The panel (a) corresponds to the evolution of a galaxy with the H I column density inside it equal to $N_{\rm H\,I} = 10^{20}$ cm^{-2}; the panel (b), to the evolution of a galaxy with the H I column density $N_{\rm H\,I} = 10^{19}$ cm^{-2} and without x-ray binaries; the panel (c), to the evolution of a galaxy with the H I column density $N_{\rm H\,I} = 10^{20}$ cm^{-2} and the contribution of x-ray binaries equal to $f_X = 0.3$. The panel (d) shows the evolutionary (i.e., redshift) dependence of the maximum brightness temperature in the H I 21-cm line as a function of galactocentric distance where this maximum brightness temperature is reached for models with $f_X = 0$ (the solid line), $f_X = 0.3$ (the dashed line), and $f_X = 1$ (the dashed-and-dotted line) for $N_{\rm H\,I} = 10^{20}$ cm^{-2} and for the model with $f_X = 0$ for $N_{\rm H\,I} = 10^{19}$ cm^{-2} (the dotted line). Redshift varies along the line and is shown by shades of gray in accordance with the scale on the right.

by shades of gray in accordance with the scale on the right. This diagram allows easy comparison of the maximum brightness temperature with the galactocentric distance where this maximum is reached and with the redshift. As is evident from the figures, the radius of the region with maximum H I 21-cm emission is the largest in the $z \sim 12.5$–11.5 redshift interval and varies from about 6 kpc for $f_X = 0$ to almost 12 kpc for $f_X = 1$ for the H I column density $N_{\rm H\,I} = 10^{20}$ cm^{-2}. The brightness temperature in the model with $f_X = 0$ in this redshift interval is equal to $\Delta T_b \sim$20–25 mK, whereas in the model with $f_X = 1$ it decreases down to almost 12–17 mK. This decrease is due to greater radius of the region in the model with more powerful x-ray radiation and hence to the corresponding decrease of the flux of $Ly\alpha$ photons.

The decrease of the absorption of ionizing photons down to $N_{\rm H\,I} = 10^{19}$ cm^{-2} in the host galaxy results in the increase of the radius of the region with maximum emission and in the broadening of the redshift interval. However, although the radius remains almost unchanged at $z \lesssim 13$, the brightness temperature decreases with redshift from about 20 mK at $z \sim 13$ down to almost 5 mK at $z \sim 11$. Thus the $z \sim 11.5$–13 redshift interval proves to be the most favorable for observations. Note that the possible extra influence of other sources of soft x-ray radiation,

e.g., black holes, hot gas, etc. [2] should contribute to the growth of the sizes and brightness temperatures.

In the models mentioned above the characteristic size (diameter) of regions with known brightness temperatures is of about 12–30 kpc, which corresponds to the angular size of $\theta \sim 0\farcm05$–$0\farcm14$ at $z \sim$ 11–12.5. The limit of sensitivity of modern radio telescopes is higher than signal levels from such objects. However, detecting them is quite a feasible task with the Square Kilometre Array (SKA) currently under construction, because the expected detection limit [42] for this telescope in observations with an angular resolution of about $0\farcm1$ at ~ 110 MHz, which corresponds to $z \sim 12$, and is equal to almost 2 mK for the band width of 30 MHz. Thus gas regions in the vicinities of dwarf galaxies with the masses and star-formation laws mentioned above can be observed in the future with SKA.

5. CONCLUSIONS

We study the effect of ionizing radiation of dwarf galaxies on the thermal and ionization state of surrounding intergalactic gas before the onset of the hydrogen reionization epoch. Ionizing photons with energies as high as several tens of eV cannot escape from the galaxy because of the high fraction of neutral gas, and only photons with energies higher than 100 eV can escape and ionize the surrounding intergalactic gas. In young galaxies at $z \sim$8–15 soft x-ray photons can be produced by hot intermediate-mass stars ($M \sim$5–8 $M_\odot$) settling on the asymptotic giant branch and massive x-ray binaries. To correctly account for the effect of the former source, we modified the spectrophotometric part of PEGASE software package, because the original spectral libraries used in it are limited to the energy of 136 eV. We use in our computations the spectral library for hot stars [25] with a much higher limiting energy. We determine the total luminosity of x-ray binaries from the empirical relation between this luminosity and star-formation rate in the galaxy [11]. Given that the effect of x-ray binaries is determined, among other factors, by the correction factor f_X, which in distant dwarf galaxies may differ from its value in the local Universe (see discussion in the text), we considered the dependence of the thermal evolution on f_X. We investigated the role of each source of radiation capable of influencing the thermal state of the intergalactic gas and computed the possible observational manifestations of the variations of this state in the H I 21-cm line. We showed that:

soft x-ray radiation from asymptotic giant branch stars can heat intergalactic gas to above 100 K and ionize it to the degree of $x_e \gtrsim 0.03$ within $r \sim$4–10 kpc around a dwarf galaxy with a mass of $6 \times 10^8\ M_\odot$ and constant burst of star formation with a rate and duration of 0.03–$0.1 M_\odot$ yr^{-1} and 100 Myr, respectively, starting at the redshift of $z \sim 15$; after the end of the burst of star formation the partially ionized regions around such galaxies remain in the quasi-stationary state over the next 200–300 Myr, i.e., up to $z \sim 7.5$;

in the case of the formation of x-ray binaries in dwarf galaxies at large redshifts the region of ionized and heated gas increases in size compared to the case where soft x-ray photons are emitted by AGB stars exclusively and the size of the corresponding region is of about 10 kpc; the increase is by a factor of 2–3 and 5–6 for $f_X = 0.1$ and $f_X \sim 1$, respectively; note that for $f_X \lesssim 0.03$ the effect of x-ray binaries proves to be comparable or weaker than from the AGB star population;

$Ly\alpha$ emission from the stellar population, heating, and ionization of the intergalactic has result in the excitation of the H I 21-cm line; the brightness temperature in the vicinity of galaxies at end of the burst of star formation is equal to about 15–25 mK at redshifts $z \sim 12.5$–11.5, and then decreases down to several mK by $z \lesssim 10$; the size of the region where the brightness temperature remains close to its maximum value is of about 12–30 kpc at $z \sim 12.5$–11.5; this corresponds to the angular size of $\theta \sim 0\farcm05$–$0\farcm14$ for the factor $f_X \sim 0 - 1$ (zero value means that x-ray photons are produced by AGB stars exclusively). Thus in the redshift interval $z \sim 12.5$–11.5 the size of the region of maximum brightness temperature is the greatest during the evolution of the dwarf galaxy and hence this period is most favorable for observations; gas regions in the vicinity of dwarf galaxies with the masses and star-formation law mentioned above can be detected with the Square Kilometre Array (SKA) currently under construction.

The estimates that we report in this paper are based on a number of assumptions about the evolution of dwarf galaxies and contain uncertain parameters including such quantities as the star-formation rate, parameter f_X characterizing the x-ray efficiency of star formation due to x-ray stars, which are critically important for our conclusions. In view of this circumstance we varied the necessary parameters from extremely conservative values (e.g., models with $f_X = 0$) to optimistic choices (such as models with $f_X \sim 1$). In all cases the corresponding interval of brightness temperature in the H I 21-line proves to be quite promising for possible signal detection with instruments currently under construction.

ACKNOWLEDGMENTS

E.O.V. is grateful to Valery Suleimanov for valuable discussions of the stellar spectra. This work was supported by the Pe joint grant by the Russian Foundation for Basic Research and Department of Science and Technology of India through project no. RFBR 17-52-45063 and DNT P-27. The development of the software package for modeling the thermal evolution was supported by the Russian Science Foundation (project no. 14-50-00043). M.V.R. acknowledges the support from the Ministry of Education and Science of the Russian Federation (project no. 3.858.2017/4.6). Yu.A.Shch. acknowledges the support from the Presidium of the Russian Academy of Sciences (project code 28).

REFERENCES

1. M. Ricotti and J. P. Ostriker, Monthly Notices Royal Astron. Soc. **352**, 547, (2004).
2. M. B. Eide, L. Graziani, B. Ciardi, et al., Monthly Notices Royal Astron. Soc. **476**, 1174, (2018).
3. B. B. Nath and P. L. Biermann, Monthly Notices Royal Astron. Soc. **265**, 241 (1993).
4. E. O. Vasiliev and Yu. A. Shchekinov, Astronomy Reports **50**, 778 (2006).
5. J. Jasche, B. Ciardi, and T. A. Ensslin, Monthly Notices Royal Astron. Soc. **380**, 417 (2007).
6. S. Sazonov and R. Sunyaev, Monthly Notices Royal Astron. Soc. **454**, 3464 (2015).
7. S. Kasuya, M. Kawasaki, and N. Sugiyama, Phys. Rev. D **69b**, 3512 (2004).
8. X. Chen and M. Kamionkowski, Phys. Rev. D **70d**, 3502 (2004).
9. M. Mapelli, A. Ferrara, and E. Pierpaoli, Monthly Notices Royal Astron. Soc. **369**, 1719 (2006).
10. A. Loeb and R. Barkana, Annual Rev. Astron. Astrophys. **39**, 19 (2001).
11. M. Gilfanov, H.-J. Grimm, and R. Sunyaev, Monthly Notices Royal Astron. Soc. **347**, L57 (2004).
12. M. Mori, A. Ferrara, and P. Madau, Astrophys. J. **571**, 40 (2002).
13. T. Kitayama and N. Yoshida, Astrophys. J. **630**, 675 (2005).
14. E. O. Vasiliev, E. I. Vorobyov, and Yu. A. Shchekinov, Astron. and Astrophys. **489**, 505 (2008).
15. Z. Haiman, A. A. Thoul, and A. Loeb, Astrophys. J. **464**, 523, (1996).
16. M. Tegmark, J. Silk, M. J. Rees, et al., Astrophys. J. **474**, 1 (1997).
17. Yu. A. Shchekinov and E. O. Vasiliev, Monthly Notices Royal Astron. Soc. **368**, 454 (2006).
18. E. Ripamonti, Monthly Notices Royal Astron. Soc. **376**, 709 (2007).
19. E. O. Vasiliev, E. I. Vorobyov, E. E. Matvienko, et al., Astronomy Reports **56**, 895 (2012).
20. M. Jeon, A. H. Pawlik, V. Bromm, and M. Milosavljević, Monthly Notices Royal Astron. Soc. **444**, 3288 (2014).
21. E. Tolstoy, V. Hill, and M. Tosi, Annual Rev. Astron. Astrophys. **47**, 371 (2009).
22. M. Fioc and B. Rocca-Volmerange, Astron. and Astrophys. **326**, 950 (1997).
23. M. Mateo, Annual Rev. Astron. Astrophys. **36**, 435 (1998).
24. R. E. S. Clegg and D. Middlemass, Monthly Notices Royal Astron. Soc. **228**, 759 (1987).
25. T. Rauch, Astron. and Astrophys. **403**, 709 (2003).
26. S. Mineo, M. Gilfanov, and R. Sunyaev, Monthly Notices Royal Astron. Soc. **426**, 1870 (2012).
27. E. Treister, K. Schawinski, M. Volonteri, et al., Nature **474**, 356 (2011).
28. S. Sazonov and I. Khabibullin, Monthly Notices Royal Astron. Soc. **476**, 2530 (2018).
29. D. Whalen, T. Abel, and M. L. Norman, Astrophys. J. **610**, 14, (2004).
30. T. Kitayama, N. Yoshida, H. Susa, and M. Umemura, Astrophys. J. **613**, 631, (2004).
31. E. O. Vasiliev, E. I. Vorobyov, A. O. Razoumov, and Yu. A. Shchekinov, Astronomy Reports **56**, 564, (2012).
32. B. Ciardi and A. Ferrara, Space Sci. Rev. **116**, 625, (2005).
33. R. Cen, Astrophys. J. Suppl. **78**, 341 (1992).
34. S. C. O. Glover and A.-K. Jappsen, Astrophys. J. **666**, 1, (2007).
35. M. Ricotti, N. Y. Gnedin, and J. M. Shull, Astrophys. J. **575**, 33, (2002).
36. J. M. Shull and M. E. van Steenberg, Astrophys. J. **298**, 268, (1985).
37. S. Seager, D. Sasselov, and D. Scott, Astrophys. J. Suppl. **128**, 407, (2000).
38. S. Yu. Sazonov and I. I. Khabibullin, Astronomy Letters **43**, 211 (2017).
39. G. B. Field, Proc. IRE **46**, 240 (1958).
40. S. Wouthuysen, Astron. J. **57**, 31 (1952).
41. X. Chen and J. Miralda-Escudé, Astrophys. J. **602**, 1 (2004).
42. S. R. Furlanetto, S. P. Oh, and F. H. Briggs, Physics Reports **433**, 181 (2006).
43. M. Kuhlen, P. Madau, and R. Montgomeri, Astrophys. J. Lett. **637**, 1 (2006).
44. H. Liszt, Astron. and Astrophys. **371**, 698 (2001).
45. X. Chen and J. Miralda-Escudé, Astrophys. J. **684**, 18 (2008).
46. M. Valdés and A. Ferrara, Monthly Notices Royal Astron. Soc. Lett. **387**, 8 (2008).

Translated by A. Dambis